# Navigation Under GNSS Denied Environments: Zero Velocity and Zero Turning Update

Oğuzhan Çifdalöz[*]

[*] Çankaya Üniversitesi, Mühendislik Fakültesi, Elektrik-Elektronik Müh. Bölümü, Ankara, Türkiye, (ORCID: 0000-0003-0523-946X), oguzhanc@cankaya.edu.tr

**Abstract**

The objective of this paper is to present a method which bounds the error of an inertial navigation system (INS) when Global Navigation Satellite System (GNSS) is not available. Inertial navigation systems utilize gyroscopes and accelerometers, and calculate velocity, position and attitude, essentially by integrating the measurements obtained from these sensors. Due to the nature of integration, INS are notoriously prone to sensor biases and drifts. Typically, GNSS is used to correct the navigation system errors caused by the inertial sensor measurements. However, in GNSS degraded or denied environments, alternative solutions are required. If the platform on which an INS is mounted is known or estimated to be stationary, zero-velocity update (ZUPT) and/or zero turning update (ZTUPT) algorithms can be applied in order to bound the navigation system errors. Under certain assumptions, ZUPT based algorithms can be applied when the platform is not stationary. If a vehicle's motion is constrained by the design of its kinematics, i.e. if it can be assumed that the vehicle cannot move or rotate along one or more of its body axes, ZUPT assisted Kalman estimators can be used to correct the errors along those axes. Potentially, ZUPT based estimation algorithms can also be utilized when a sufficiently high fidelity vehicle model is available. In this paper, the implementation of zero-velocity update (ZUPT) and zero turning update (ZTUPT) algorithms are analyzed for the purpose of estimating and bounding inertial navigation errors. The basic principle in navigation is based on combining the data obtained from the sensors onboard and the inertial navigation system through an Extended Kalman filter. Although this process requires additional software components, it potentially offers increased system accuracy and reliability. Incorporating the kinematics of the vehicle, along with a ZUPT and/or ZTUPT algorithm, provides additional data to feed into the Kalman filter and increases the efficiency of error estimation. Estimated error is then fed back into the INS algorithm in order to counteract the sources of error.

**Keywords:** Inertial Navigation Systems, Zero Velocity Update, Zero Turn Update, Extended Kalman Filters.

# Küresel Konumlama Sisteminin Olmadığı Ortamlarda Navigasyon: Sıfır Hız ve Sıfır Dönü Güncelleme

**Öz**

Bu makalenin amacı, Küresel Konumlama Sisteminin (KKS) mevcut olmadığı durumlarda, bir ataletsel navigasyon sisteminin hata sinyallerini sınırlandırmayı amaçlayan bir yöntem sunmaktır. Ataletsel navigasyon sistemleri (ANS) dönüölçer ve ivmeölçerleri kullanır ve –özde– bu algılayıcılardan elde edilen sinyallerinin integralini alınarak hız, konum ve yönelimi hesaplar. Integral alma işleminin doğası gereği ANS, algılayıcıların kaymalarına ve sapmalarına karşı son derece hassastır. Tipik olarak, KKS, ataletsel algılayıcı ölçümlerinin neden olduğu navigasyon sistemi hatalarını düzeltmek için kullanılır. Ancak, KKS'nin kalitesinin bozulduğu veya KKS verisinin erişilir olmadığı ortamlarda alternatif çözümler gereklidir. Eğer bir ANS'nin monte edildiği platformun hareketsiz olduğu biliniyor veya tahmin ediliyor ise, navigasyon sistemi hatalarını sınırlandırmak amacıyla, sıfır hız güncellemesi (ZUPT) ve sıfır dönü güncellemesi (ZTUPT) algoritmaları uygulanabilir. Belirli varsayımlar altında, platformun durağan olmadığı durumlarda da ZUPT tabanlı algoritmalar uygulanabilir. Eğer bir aracın hareketi, kinematiğinin tasarımı ile sınırlıysa, yani aracın hareket edemeyeceği veya dönemeyeceği bir veya daha fazla eksen varsa, ZUPT destekli Kalman filtre algoritmaları bu eksenler doğrultusundaki hataları düzeltmek için kullanılabilir. Potansiyel olarak, ZUPT tabanlı tahmin algoritmaları, yeterince yüksek sadakatli bir araç modeli mevcutsa da kullanılabilir. Bu makalede, sıfır hız güncellemesi (ZUPT) ve/veya sıfır dönü güncellemesinin uygulanması yoluyla ataletsel navigasyon sistemi hatalarının tahmin edilmesi ve sınırlandırılması konusu incelenmektedir. Navigasyondaki temel prensip, platform üzerindeki algılayıcılardan elde edilen verilerin bir Genişletilmiş Kalman filtresi aracılığıyla ataletsel navigasyon sistemine entegre edilmesine dayanır. Bu işlem ek yazılım bileşenleri gerektirse de, potansiyel olarak artan bir doğruluk ve güvenilirlik sunar. Sıfır hız ve sıfır dönü algoritmalarına araç kinematiklerinin de eklenmesi, Kalman filtreye ek veri sağlar ve hata tahmininin doğruluğunu artırır. Tahmin edilen hata ANS algoritmasına geri beslenerek hata kaynaklarının etkisinin azaltılması sağlanır.

**Anahtar Kelimeler:** Ataletsel Navigasyon Sistemleri, Sıfır Hız Güncelleme, Sıfır Dönü Güncelleme, Genişletilmiş Kalman Filtre.

[*] Sorumlu Yazar: oguzhanc@cankaya.edu.tr

# 1. Introduction

An inertial navigation system (INS) is comprised of an inertial measurement unit (IMU), aiding sensors and a sensor/data fusion algorithm. In the case where the aiding system is a global navigation satellite system (GNSS), an integrated INS/GNSS provides absolute position and attitude information (Titterton and Weston, 2004). When GNSS is unavailable, denied or degraded due to jamming, disturbances, or physical conditions, external aiding sensors and systems are required in order to bound the position, velocity and attitude errors of an INS (Schmidt, 2015). Accelerometers and gyroscopes in an IMU are subject to numerous error sources such as bias, scale factor, nonlinearities, dead zone, quantization, and bandwidth limitations. Since computing position, velocity and attitude is performed essentially by integrating the measurements obtained from these sensors, the navigation solution will diverge from the true solution.

The objective of this study is to provide an extended Kalman filter based algorithm that can be utilized in order to bound navigation errors. Specifically, zero velocity update (ZUPT) and zero turning update (ZTUPT) methods are investigated (Akcayir and Ozkazanc, 2003). Hence, in this study, the vehicle is assumed to be stationary in a GNSS denied environment. Various methods are proposed for zero velocity detection (Wagstaff and Kelly, 2018), (Wahlström et al., 2019), (Xiaofang et al., 2014), and it is outside the scope of this study.

Determining position and attitude when a vehicle is at rest is crucial in military applications. US Army's Bradley Fighting Vehicle and Turkish Fırtına (Figures 1 and 2) are some of the leading examples of such vehicles.



*Figure 1. Bradley Fighting Vehicle*



*Figure 2. T-155 Fırtına Howitzer*

For high precision target engagement, these vehicles require high fidelity position and attitude (angular orientation) information under conditions where GNSS is not available.

Navigation equations are highly nonlinear. They need to be linearized in order to implement an extended Kalman filter for state estimation. This is performed by approximating the nonlinear state equations, implemented either in Euler angles or quaternions, by a piece-wise constant system (PWCS) at each iteration. Approximating the nonlinear system at the current iteration's state-input combination helps capture the characteristic behavior of the system with little loss of accuracy (Goshen-Meskin and Bar-Itzhack, 1992a,b).

Through this implementation, expected outputs (zero velocity and/or zero turning) of a stationary vehicle and the outputs of the navigation equations are contrasted to obtain estimates of the navigation error states. In this sense, the control system is an output feedback controller. Error states are fed back to the navigation equations for the purposes of bounding INS errors, and simultaneously, estimating sensor drifts and biases.

The remainder of the paper is structured as follows: Section 2 states the problem to be addressed and describes the navigation system model, Section 3 describes the proposed solution and includes two scenarios, and finally Section 4 summarizes the paper and presents future directions.

# 2. Problem Statement and Model

The problem that needs to be addressed is the determination of position and attitude (Euler angles) of a vehicle, when it is not moving linearly. When GNSS is available, latitude ($L$), longitude ($\lambda$), altitude ($h$), north velocity ($v_N$), east velocity ($v_E$), down velocity ($v_D$), roll angle ($\varphi$) and pitch angle ($\theta$) can be obtained with very high accuracy. When GNSS is jammed or becomes unavailable for any reason, inertial sensors and other sensors such as barometers and magnetometers can be used. Although these sensors require no other external information source, their measurements are prone to measurement noise, biases, and drifts.

Inertial navigation systems utilize a variety of sensors such as gyroscopes, accelerometers, magnetometers and barometers in order to compute velocity, position and attitude, essentially by integrating the measurements obtained from these sensors. Integration results in the problem of drifts in the solution, due to the biases and noise characteristics of these sensors. Typically, sensors which provide accurate position information are used in order to correct the navigation solution. A very common sensor is the GNSS. However, in environments where GNSS data are not available or degraded, alternative solutions are required.

A side note should be given here for the heading angle: Determining the heading angle ($\psi$) is more complicated because it is closely associated with the North Finding Problem (Titterton and Weston, 2004). Magnetometers may be helpful, however, it should be noted that magnetometers will yield the magnetic north, which is different than the geodetic (true) north. True north can be determined by very high accuracy and low noise gyroscopes (expensive), or by using lower accuracy sensors. Lower accuracy sensor outputs may need to be collected for long periods of time for averaging (Titterton and Weston, 2004). North finding is left outside scope of this study and the effect of this exclusion will be apparent in the simulations results given in the following sections.

In order to describe the method devised to bound inertial navigation errors, navigation equations need to be described.

## 2.1. Navigation Equations

Navigation equations are nonlinear differential equations which define the position, velocity, and the attitude of the navigation system. They consist of three highly coupled components: *(i)* a set of equations to compute latitude, longitude, and altitude ($L$, $\lambda$, $h$), *(ii)* another set of equations to compute the north, east and down velocities in the navigation frame ($v_N$, $v_E$, $v_D$), and *(iii)* another set of equations to compute attitude, i.e. the roll, pitch and yaw Euler angles ($\varphi$, $\theta$, $\psi$). Notation and terminology used throughout the document is due to (Titterton and Weston, 2004).

Throughout the document references are made to the reference coordinate frames (Groves, 2013). *Inertial frame* is a non-rotating frame with respect to the fixed stars with origin at the center of the Earth and *z*-axis along the Earth's polar axis. *Navigation frame* is local geographic frame. Its origin is located on the navigating platform and the axes are aligned with north, east, and down. Navigation frame is tangent to the surface of the Earth. *Body frame* also has its origin on the navigating platform (usually at its center of gravity), and the axes are aligned with the Euler angles of the platform.

Gyroscopes measure the angular rate of the body frame with respect to the inertial frame as resolved in the body frame and are given by

$$\omega_{ib}^b = \begin{bmatrix} \omega_x \\ \omega_y \\ \omega_z \end{bmatrix}$$

where $\omega_x$, $\omega_y$, and $\omega_z$ denote the measurements obtained from a gyroscope's $x$, $y$, $z$ axes, respectively.

In order to compute the Euler angles, one needs the angular rate of the body frame with respect to the navigation frame as resolved in the body frame given as

$$\omega_{nb}^b = \omega_{ib}^b - C_n^b(\omega_{ie}^n + \omega_{en}^n) \qquad (1)$$

where

$$\omega_{ie}^n = \begin{bmatrix} \Omega \cos L \\ 0 \\ -\Omega \sin L \end{bmatrix} \qquad (2)$$

denotes the turn rate of the earth, and

$$\omega_{en}^n = \begin{bmatrix} \dfrac{v_E}{R+h} \\ -\dfrac{v_N}{R+h} \\ -\dfrac{v_E \tan L}{R+h} \end{bmatrix} \qquad (3)$$

denotes the turn rate of the navigation frame, *the transport rate*, due to its $v_N$, north velocity, $v_E$, east velocity, and $v_D$, down

velocity on Earth. In Equations 1, 2, and 3, $R$ denotes the mean radius of the earth, $L$ the latitude, $h$ the height above ground, $\Omega$ the turn rate of the Earth, and $C_n^b$ denotes the transformation matrix from the navigation frame to the body frame.

The transformation matrix from the body frame to the navigation frame $C_b^n = (C_n^b)^T$ is given (for Euler angle implementation) by (Titterton and Weston, 2004)

$$C_b^n = \begin{bmatrix} C_\psi C_\theta & C_\psi S_\theta S_\phi - S_\psi C_\phi & C_\psi S_\theta C_\phi + S_\psi S_\phi \\ S_\psi C_\theta & S_\psi S_\theta S_\phi + C_\psi C_\phi & S_\psi S_\theta C_\phi - C_\psi S_\phi \\ -S_\theta & C_\theta S_\phi & C_\theta C_\phi \end{bmatrix}$$

where $C_x \triangleq \cos x$ and $S_x \triangleq \sin x$.

The first set of equations, so-called *the kinematic equation,* is used to compute the Euler angles from the body angular rates measured by the gyroscope, and is given by

$$\begin{bmatrix} \dot\phi \\ \dot\theta \\ \dot\psi \end{bmatrix} = \begin{bmatrix} 1 & \sin\phi \tan\theta & \cos\phi \tan\theta \\ 0 & \cos\phi & -\sin\phi \\ 0 & \sin\phi/\cos\theta & \cos\phi/\cos\theta \end{bmatrix} \omega_{nb}^b. \qquad (4)$$

The second set of navigation equations are associated with the north, east, down velocities of the navigation system (frame), given by

$$\begin{bmatrix} \dot v_N \\ \dot v_E \\ \dot v_D \end{bmatrix} = \mathbf{C}_b^n \mathbf{f}^b - (2\omega_{ie}^n + \omega_{en}^n) \times \begin{bmatrix} v_N \\ v_E \\ v_D \end{bmatrix} + \begin{bmatrix} 0 \\ 0 \\ g(h) \end{bmatrix} \qquad (5)$$

where, assuming a perfectly spherical earth,

$$g(h) = \frac{g_0}{\left(1 + \dfrac{h}{R}\right)^2}.$$

In Equation 5, $g_0$ denotes the gravitational acceleration of the Earth and $\mathbf{f}^b$ denotes the accelerometer measurements, i.e.

$$\mathbf{f}^b = \begin{bmatrix} f_x \\ f_y \\ f_z \end{bmatrix}$$

where $f_x$, $f_y$, and $f_z$ denote the measurements obtained from an accelerometer's $x$, $y$, $z$ axes, respectively.

The third set of navigation equations are associated with the geographic coordinates and altitude. It is given by

$$\begin{bmatrix} \dot L \\ \dot \lambda \\ \dot h \end{bmatrix} = \begin{bmatrix} \frac{1}{R+h} & 0 & 0 \\ 0 & \frac{\sec L}{R+h} & 0 \\ 0 & 0 & -1 \end{bmatrix} \begin{bmatrix} v_N \\ v_E \\ v_D \end{bmatrix}. \qquad (6)$$

Equations 4, 5, and 6 can be combined to form a first order nonlinear differential equation to represent the navigation equation such that

$$\dot{x}^* = f^*(x^*, u^*) \tag{7}$$

where

$$x^* \triangleq \begin{bmatrix} L & \lambda & h & v_N & v_E & v_D & \phi & \theta & \psi \end{bmatrix}^T$$

denotes the navigation state vector, and

$$u^* \triangleq \begin{bmatrix} f_x & f_y & f_z & \omega_x & \omega_y & \omega_z \end{bmatrix}^T$$

denotes input vector, i.e. the vector of inertial measurement unit (IMU) measurements.

A more complete and comprehensive model can be formed by augmenting Equation 7 by 6 decoupled differential equations in order to include the inertial sensor errors, specifically accelerometer drifts and the gyroscope biases. Hence, the state vector is augmented to be

$$x \triangleq \begin{bmatrix} L & \lambda & h & v_N & v_E & v_D & \phi & \theta & \psi & d_x & d_y & d_z & b_x & b_y & b_z \end{bmatrix}^T$$

where $d_*$ are the accelerometer drifts and $b_*$ are the gyroscope biases for each axis. The added differential equations are

$$\begin{aligned}
\dot{d}_x &= 0, & d_x(0) &= \bar{d}_x \\
\dot{d}_y &= 0, & d_y(0) &= \bar{d}_y \\
\dot{d}_z &= 0, & d_z(0) &= \bar{d}_z \\
\dot{b}_x &= 0, & b_x(0) &= \bar{b}_x \\
\dot{b}_y &= 0, & b_y(0) &= \bar{b}_y \\
\dot{b}_z &= 0, & b_z(0) &= \bar{b}_z
\end{aligned}$$

in which the initial conditions denote the constant residual drift error of the accelerometer and gyroscope. The IMU readings are then modified to include these errors, i.e.

$$u \triangleq \begin{bmatrix} f_x + d_x & f_y + d_y & f_z + d_z & \omega_x + b_x & \omega_y + b_y & \omega_z + b_z \end{bmatrix}^T$$

Finally, we arrive at the 15-dimensional nonlinear navigation equations in the form of Equation 8.

$$\dot{x} = f(x, u) \tag{8}$$

## 2.2. Navigation Errors

Inertial navigation dynamics (Equation 8) are unstable (Groves, 2013), i.e. its solution diverges in time when no aiding (correcting) sensor output is available.

In the simulations below, the vehicle is assumed to be equipped with a tactical grade inertial measurement unit (IMU). The accelerometer bias is assumed to be *1 mg (1σ)* and gyroscope bias is assumed to be *1 deg/hr (1σ)*. These values are typical for a tactical grade IMU. Bias instability is ignored.

Consider that this vehicle loses access to the GNSS, at which time its geodetic coordinates, altitude and attitude (i.e. Euler angles) are

$$\begin{bmatrix} L \\ \lambda \\ h \end{bmatrix} = \begin{bmatrix} 40° \\ 33° \\ 200\ m \end{bmatrix} \text{ and } \begin{bmatrix} \phi \\ \theta \\ \psi \end{bmatrix} = \begin{bmatrix} 5° \\ 10° \\ 15° \end{bmatrix} \tag{9}$$

and its velocity vector is

$$\begin{bmatrix} v_N \\ v_E \\ v_D \end{bmatrix} = \begin{bmatrix} 0 \\ 0 \\ 0 \end{bmatrix}.$$

Given the above, using Equations 1, 5 and 9, ideal (no bias, no noise) accelerometer measurements can be computed as

$$\begin{bmatrix} f_x \\ f_y \\ f_z \end{bmatrix} = \begin{bmatrix} -g \sin\theta \\ g \cos\theta \sin\phi \\ g \cos\theta \cos\phi \end{bmatrix} = \begin{bmatrix} 0.855 \\ -1.697 \\ -9.6242 \end{bmatrix} m/s^2 \tag{10}$$

and the ideal gyroscope measurements can be computed as

$$\begin{bmatrix} \omega_x \\ \omega_y \\ \omega_z \end{bmatrix} = C_n^b \begin{bmatrix} \Omega \cos L \\ 0 \\ -\Omega \sin L \end{bmatrix} = \begin{bmatrix} 0.00033048 \\ -0.0012302 \\ -0.0022195 \end{bmatrix} deg/s \tag{11}$$

The *ideal* measurements given in Equations 10 and 11 are dubbed as such because these sensor outputs (when there is no noise or bias) results in

$$f(x, u) = 0,$$

i.e. the navigation solution is exact. However, in the simulations below, the ideal measurements given in Equations 10 and 11 are corrupted by bias and noise (with variances of 1/10 of the bias variances) in order to compute the navigation errors when noise and bias exists in the system. So, the following results demonstrate a typical navigation solution without GNSS or any other aiding sensor, such as a barometer or a magnetometer.
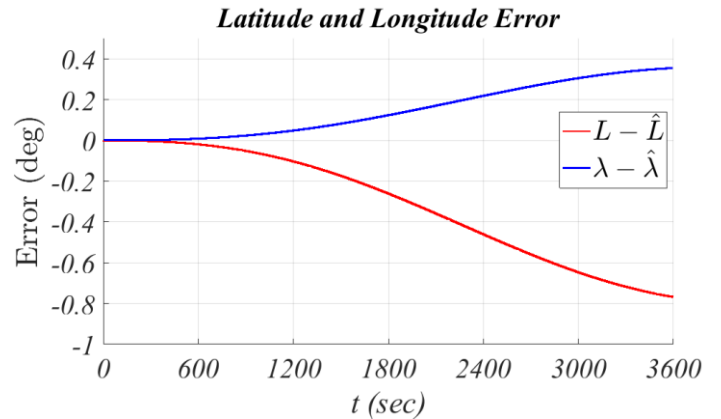


*Figure 3. Latitude and Longitude Error*

Figure 3 shows the latitude and longitude errors. About *-0.8°* of drift for the latitude and about *0.35°* of drift of longitude correspond to approximately 90 kilometers of position error in one hour. This performance is typical of a tactical grade IMU. The relative boundedness of these errors are due to the well-known Schuler Pump mechanism.
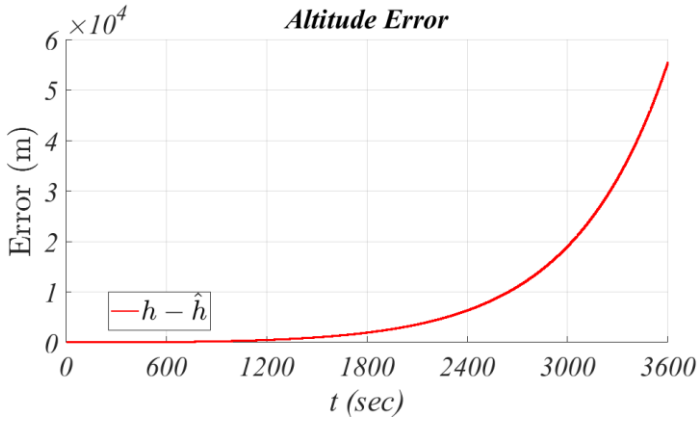
*Figure 4. Altitude Error*

Figure 4 indicates that a much severe error accumulates for the altitude. Altitude channel is particularly sensitive to drifts and biases of the IMU (Groves, 2013, pp.231).
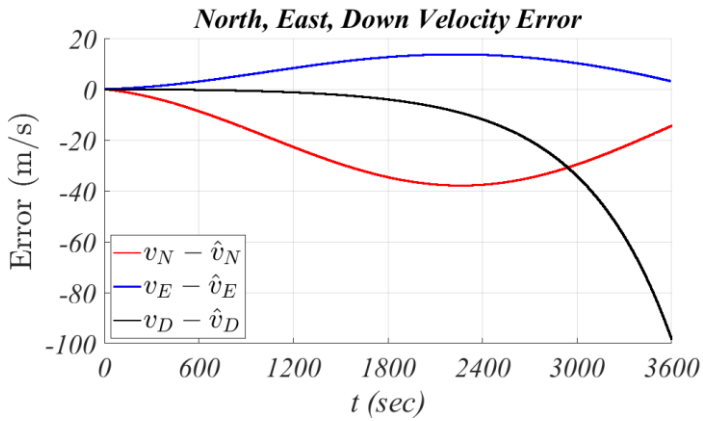


*Figure 5. North, East, Down Velocity Error*

Figure 5 indicates that the error for north, east, and down velocities are considerably large. Down velocity is more sensitive to IMU errors. This sensitivity is exaggerated by the altitude channel. Note that by Equation 6, altitude is the negative integral of down velocity.
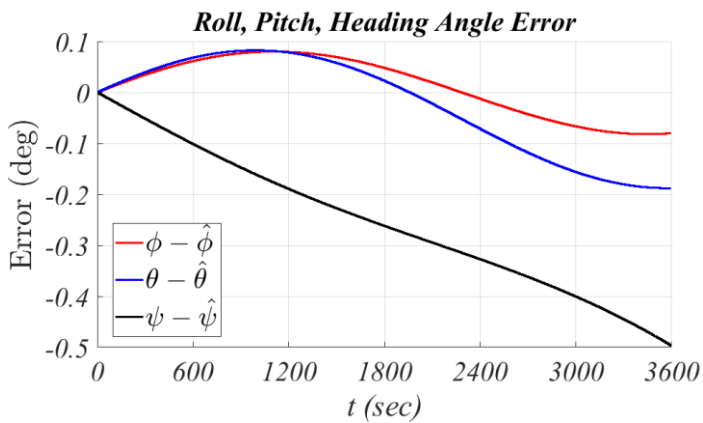


*Figure 6. Roll, Pitch, Heading Angle Error*

Figure 6 shows that the attitude solution of the navigation equations are not as large after one hour compared to the other navigation states. This is due to the fact that angular rates obtained from a gyroscope is integrated once to obtain Euler angles (Equation 4), while accelerometer outputs are integrated twice in order to obtain positon (Equations 5 and 6). Nevertheless, since the navigation equations are highly coupled, even small errors in

the Euler Angles will have a large impact on the remaining states. It is also apparent that the heading channel is more sensitive to measurement errors.

The above results show that the error of the navigation solution of a tactical grade IMU is intolerably large, if the solution is not corrected by an aiding sensor or an algorithm. 90 kilometers of positional error and 10s of kilometers of altitude error give a clear sign that the absence of GNSS drives the error to unacceptable levels and that alternative strategies are needed.

## 3. Proposed Solution and Results

In this paper, INS errors are aimed to be bounded by utilizing an Extended Kalman Filter (EKF) along with the information that the vehicle in consideration is stationary. Figure 7 describes the EKF process. EKF is considered as a standard in the theory of nonlinear state estimation and navigation systems (Julier and Uhlmann, 2004), (Musoff and Zarchan, 2009), (Wan, 2006).
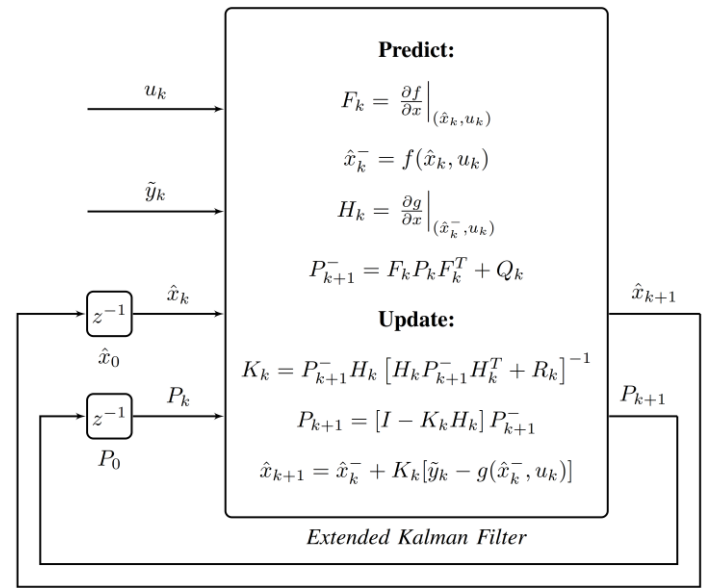


*Figure 7. Extended Kalman Filter Structure*

In Figure 7,

- $u_k = [f_x \ f_y \ f_z \ \omega_x \ \omega_y \ \omega_z]_k^T$ denotes the IMU measurements,
- $\hat{x}_k = [L \ \lambda \ h \ v_N \ v_E \ v_D \ \phi \ \theta \ \psi \ d_x \ d_y \ d_z \ b_x \ b_y \ b_z]_k^T$ denotes the current estimate (computed) of the navigation states,
- $\hat{x}_{k+1}$ denotes the next estimate of the navigation states,
- $f(x, u)$ denotes the navigation equations described in Equations 1 - 8,
- $g(x, u)$ denotes the output function, which usually is simply a state selector,
- $\tilde{y}_k$ denotes the auxiliary inputs, such as outputs of an assisting sensor, or derived information,
- $Q_k$ and $R_k$ denote the extended Kalman filter design parameters (covariance matrices),
- $F_k$ and $H_k$ denote the discrete state space matrices of the linearized navigation dynamics (explained below),
- $P_k$ and $P_{k+1}$ denote the current and next covariance matrices of the Kalman solution, respectively, and
- $K_k$ denotes the extended Kalman filter gain.

In order to employ the Extended Kalman Filter (EKF), state equations need to be linearized at each time instant when a new measurement becomes available. Given

$$\dot{x} = f(x, u), \quad x(0) = x_o \tag{12}$$

$$y = g(x, u) \tag{13}$$

Such that $x \in \mathbb{R}^n$, $x_o \in \mathbb{R}^n$, $u \in \mathbb{R}^m$, $y \in \mathbb{R}^p$, $f(x, u) \in \mathbb{R}^n$, $g(x, u) \in \mathbb{R}^p$, where $n$ is the number of states, $m$ is the number of inputs, and $p$ is the number of outputs. Described below is the process by which a linear state space representation of a nonlinear system is derived.

Linearization of Equations 12 and 13 about a fixed point $(x_*, u_*)$ is obtained as follows. Defining small perturbations

$$\delta x(t) \triangleq x(t) - x_* \quad \text{and} \quad \delta u(t) \triangleq u(t) - u_*$$

a small signal linear state-space representation is obtained as:

$$\delta \dot{x}(t) = \mathbf{A} \delta x(t) + \mathbf{B} \delta u(t) \tag{14}$$

$$y(t) = \mathbf{C} \delta x(t) + \mathbf{D} \delta u(t) \tag{15}$$

where

$$\mathbf{A} = \left. \frac{\partial f}{\partial x} \right|_{(x_*, u_*)} \triangleq \begin{bmatrix} \frac{\partial f_1}{\partial x_1} & \cdots & \frac{\partial f_1}{\partial x_n} \\ \vdots & \ddots & \vdots \\ \frac{\partial f_n}{\partial x_1} & \cdots & \frac{\partial f_n}{\partial x_n} \end{bmatrix}_{(x_*, u_*)}$$

$$\mathbf{B} = \left. \frac{\partial f}{\partial u} \right|_{(x_*, u_*)} \triangleq \begin{bmatrix} \frac{\partial f_1}{\partial u_1} & \cdots & \frac{\partial f_1}{\partial u_m} \\ \vdots & \ddots & \vdots \\ \frac{\partial f_n}{\partial u_1} & \cdots & \frac{\partial f_n}{\partial u_m} \end{bmatrix}_{(x_*, u_*)}$$

$$\mathbf{C} = \left. \frac{\partial g}{\partial x} \right|_{(x_*, u_*)} \triangleq \begin{bmatrix} \frac{\partial g_1}{\partial x_1} & \cdots & \frac{\partial g_1}{\partial x_n} \\ \vdots & \ddots & \vdots \\ \frac{\partial g_p}{\partial x_1} & \cdots & \frac{\partial g_p}{\partial x_n} \end{bmatrix}_{(x_*, u_*)}$$

$$\mathbf{D} = \left. \frac{\partial g}{\partial u} \right|_{(x_*, u_*)} \triangleq \begin{bmatrix} \frac{\partial g_1}{\partial u_1} & \cdots & \frac{\partial g_1}{\partial u_m} \\ \vdots & \ddots & \vdots \\ \frac{\partial g_p}{\partial u_1} & \cdots & \frac{\partial g_p}{\partial u_m} \end{bmatrix}_{(x_*, u_*)}$$

**A**, **B**, **C**, **D** matrices are essentially the Jacobians of the input and output functions with respect to the states and inputs. The Extended Kalman filter is implemented in discrete time. ZOH discretization of the equations given in 14 and 15 at a sampling period of $T_s$ are ($\delta$'s are dropped for brevity)

$$x_{k+1} = \mathbf{F}_k x_k + \mathbf{G}_k u_k$$
$$y_k = \mathbf{H}_k x_k + \mathbf{N}_k u_k$$

where

$$exp \left\{ \begin{bmatrix} \mathbf{A} & \mathbf{B} \\ \mathbf{0} & \mathbf{0} \end{bmatrix} T_s \right\} = \begin{bmatrix} \mathbf{F}_k & \mathbf{G}_k \\ \mathbf{0} & \mathbf{I} \end{bmatrix},$$

$$\mathbf{H}_k = \mathbf{C}, \quad \text{and} \quad \mathbf{N}_k = \mathbf{D}.$$

Discrete state space representation of the 15-state augmented navigation system, after linearization about a fixed $(x_k, u_k)$ is given by

$$\begin{bmatrix} x_{k+1} \\ z_{k+1} \end{bmatrix} = \begin{bmatrix} \mathbf{F}_k & \mathbf{G}_k \\ \mathbf{0} & \mathbf{I} \end{bmatrix} \begin{bmatrix} x_k \\ z_k \end{bmatrix} + \begin{bmatrix} \mathbf{G}_k \\ \mathbf{0} \end{bmatrix} u_k$$

$$y_k = \begin{bmatrix} \mathbf{H}_k & \mathbf{0} \end{bmatrix} \begin{bmatrix} x_k \\ b_k \end{bmatrix} + \mathbf{N}_k u_k$$

where $z_k \triangleq [d_x \; d_y \; d_z \; b_x \; b_y \; b_z]_k^T$ denotes the inertial sensor errors.

Finally, an extended Kalman filter can be implemented (Ma et al., 2020). At each step, a Kalman gain, $K_k$, is computed and correction in state estimation is achieved (see Figure 7) by

$$\hat{x}_{k+1} = \hat{x}_k^- + K_k[\tilde{y}_k - g(\hat{x}_k^-, u_k)]$$

In the following subsections, ZUPT and ZTUPT algorithms are demonstrated on selected scenarios.

## 3.1. Zero Velocity Update (ZUPT)

Zero velocity update (ZUPT) refers to the condition that north, east, down velocities of a vehicle is known or estimated to be zero. An EKF is devised that will utilize this information in order to bound the navigation errors.

Consider the scenario described in Section 2.2. The initial navigation states given in Equation 9 constitute the initial state vector, and the initial estimate of the EKF is assumed 0. The ideal sensor outputs are given in Equations 10 and 11, and the vehicle is assumed to be equipped with a tactical grade IMU as in Section 2.2. At the initialization of the simulations, bias values are determined and are kept constant throughout the simulations.

ZUPT algorithm assumes no knowledge of the position and attitude (Euler angles) of the vehicle. The only information that is available and fed to the algorithm is

$$\tilde{y}_k = \begin{bmatrix} v_N \\ v_E \\ v_D \end{bmatrix} = \begin{bmatrix} 0 \\ 0 \\ 0 \end{bmatrix}.$$

Note that $\tilde{y}_k = 0$ is not a sensor measurement, but can be considered as a constraint. Hence, the associated covariance matrix is zero, i.e. $R_k = \mathbf{0}_{3x3}$.

Latitude and longitude errors are given in Figures 8 and 9. Although position and Euler angles are known to be not varying under the described scenario, estimation for these quantities is still required because the sensor measurements are biased.
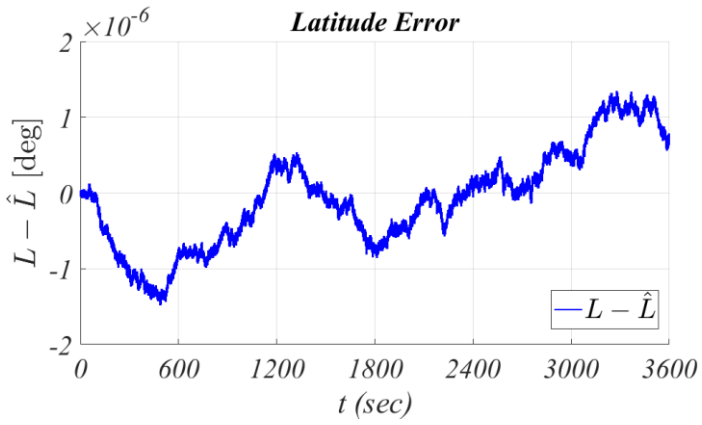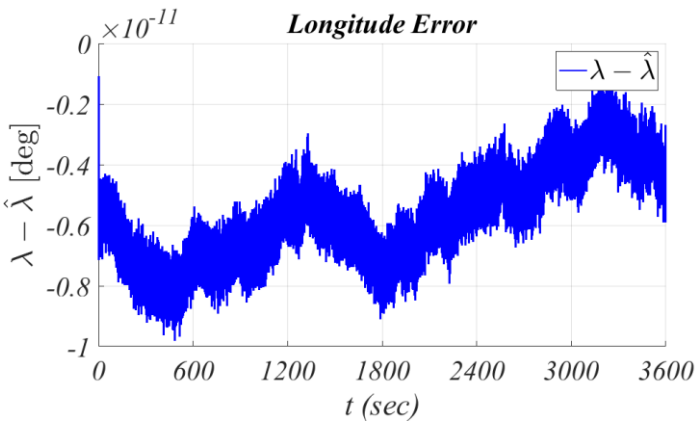
*Figure 8. Latitude Error (ZUPT case)*



*Figure 9. Longitude Error (ZUPT case)*

Figures 3 in Section 2.2 showed that, when the ZUPT algorithm is not active, latitude and longitude errors were large and resulted in a position error of approximately 90 km. However, as Figures 9 and 10 indicate, when the ZUPT algorithm is active, almost no position error is made. According to the above results, position error is less than 1 m after one hour of operation without access to GNSS.

*Note that no aiding sensor is used to achieve this result. Just the information that the vehicle is at rest results in significantly smaller navigation errors.*
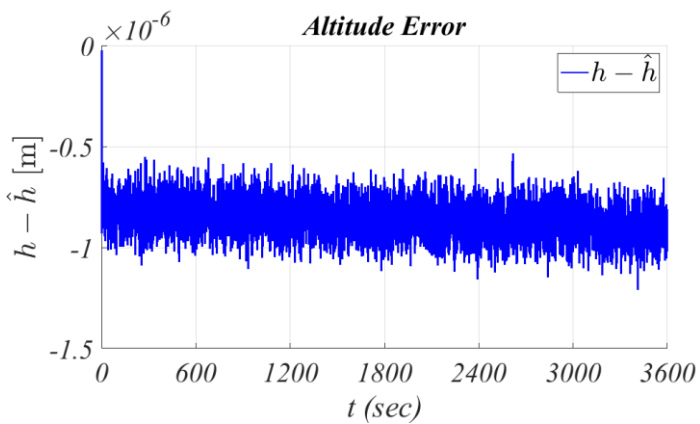


*Figure 10. Altitude Error (ZUPT case)*

It was shown previously in Figure 4 in Section 2.2 that altitude diverges when the EKF with ZUPT is not running. However, the altitude error is virtually nonexistent when the EKF with ZUPT is active (Figure 10).

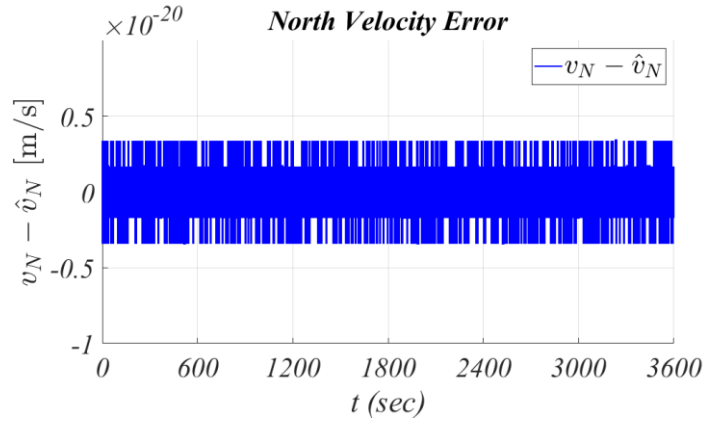Figures 11, 12, and 13 display north, east, and down velocities respectively.

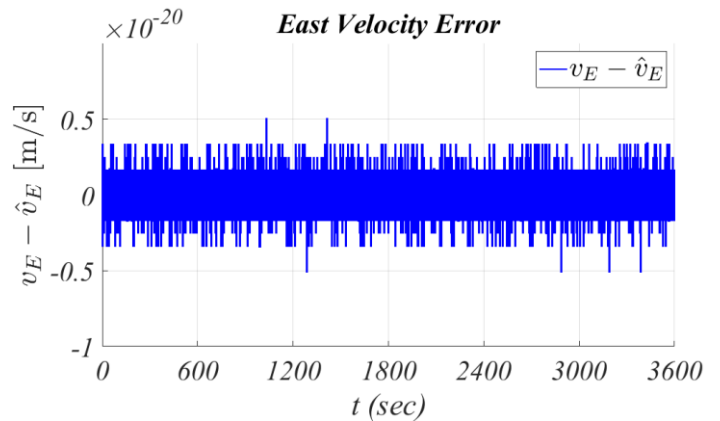

*Figure 11. North Velocity Error (ZUPT case)*



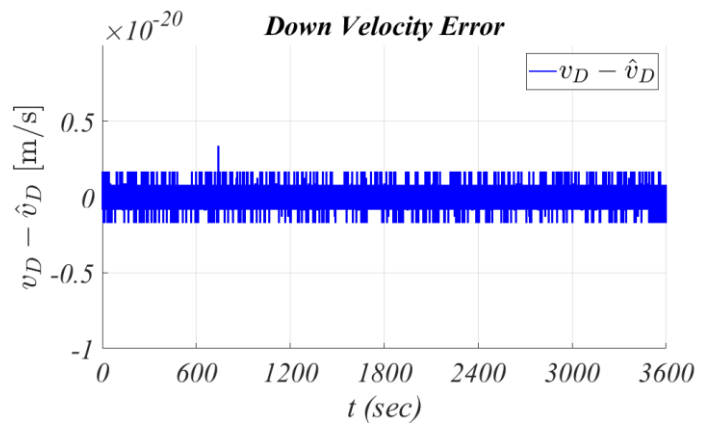*Figure 12. East Velocity Error (ZUPT case)*



*Figure 13. Down Velocity Error (ZUPT case)*

Figures 11 – 13 show that the EKF with ZUPT is performing as expected for the north, east, and down velocities. That this result is expected is due to the fact that (zero) velocities are made available to the EKF and north, east, and down velocities are enforced to remain at zero. The case where the EKF with ZUPT is not active exhibit large velocity errors (see Figure 5 in Section 2.2).

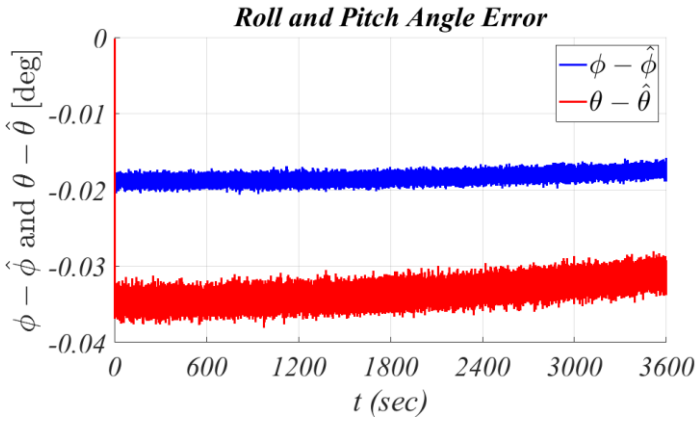Figure 14 show the roll and pitch angle errors when the EKF with ZUPT is active.

*Figure 14. Roll and Pitch Angle Errors (ZUPT case)*

Figure 14 demonstrates that the EKF with ZUPT algorithm also bounds roll and pitch angle errors, although it cannot drive them to zero. This is because the EKF is not given any information on Euler angles. Roll and pitch angles are initially computed with some error; about *-0.02°* for the roll angle and about *-0.035°* for the pitch angle. This error is due to roll and pitch rate biases of the gyroscope and the time required for the convergence of the extended Kalman filter. The smaller the bias, the smaller the error. (Note that there is no discontinuity in the computed roll and pitch angles. The seemingly discontinuous behavior is due to the time scale of the plots.) By comparison, this result is better than the scenario without the EKF as shown in Figure 6.
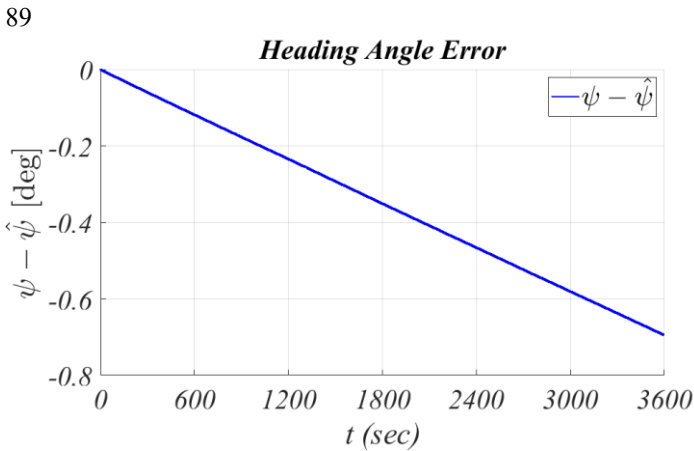
89



*Figure 15. Heading Angle Error (ZUPT case)*

Figure 15 shows that the EKF with ZUPT algorithm is completely ineffective on the heading angle. The main reason behind this result is the fact that the heading angle is an unobservable state (Titterton and Weston, 2004). It performed even worse than the nonfunctional filter scenario (see Figure 6 in Section 2.2). However, this is completely due to the random sensor noise generated in the simulation. In other simulation runs, EKF with ZUPT could be better, although that would still not negate the fact that ZUPT has no effect on the heading angle. As stated before, dedicated North Finding algorithms are devised for heading angle estimation (Titterton and Weston, 2004).

In short, ZUPT is a very successful algorithm in bounding position ($L$, $\lambda$, $h$) and velocity ($v_N$, $v_E$, $v_D$) errors. Roll and pitch angle ($\varphi$, $\theta$) errors may be considered more than acceptable, however, it is completely unreliable for the heading angle ($\psi$). This motivates the next improvement on the ZUPT method.

## 3.2. Zero Turn Update (ZTUPT)

The main invention of ZTUPT is to feed into the extended Kalman filter the additional information that a vehicle at rest is also non-rotating, i.e. its *Euler angle rates* are zero. As given in Equation 4, Euler rates evolve in time in accordance with

$$\begin{bmatrix} \dot{\phi} \\ \dot{\theta} \\ \dot{\psi} \end{bmatrix} = T\omega_{nb}^b = T(\omega_{ib}^b - C_n^b(\omega_{ie}^n + \omega_{en}^n)) \qquad (15)$$

where

$$T = \begin{bmatrix} 1 & \sin\phi\tan\theta & \cos\phi\tan\theta \\ 0 & \cos\phi & -\sin\phi \\ 0 & \sin\phi/\cos\theta & \cos\phi/\cos\theta \end{bmatrix}$$

ZTUPT utilizes the additional information that

$$\begin{bmatrix} \dot{\phi} \\ \dot{\theta} \\ \dot{\psi} \end{bmatrix} = 0 \qquad (16)$$

when a vehicle is stationary.

For Equation 15 to be equal to zero, either $T$ must be a zero matrix, which it clearly is not, or it must have a non-empty null space. For a land vehicle, it is safe to assume that $-\pi/2 < \theta < \pi/2$. Then,

$$\det(T) = \frac{1}{\cos\theta} \neq 0$$

for all $\theta \in [-\pi/2, \pi/2]$, which in turn means that the null space of T is empty, i.e.

$$\mathcal{N}(T) = \emptyset.$$

Therefore, for Equation 15 to be true, it must be that

$$\omega_{nb}^b = \omega_{ib}^b - C_n^b(\omega_{ie}^n + \omega_{en}^n) = 0.$$

However, since a vehicle at rest has zero linear velocities as well, by Equation 3, $\omega_{en}^n = 0$. This further simplifies the zero turning condition to

$$\omega_{ib}^b - C_n^b\omega_{ie}^n = 0 \qquad (17)$$

which describes what the gyroscopes should measure under such zero velocity and zero turning conditions.

In order to implement the ZTUPT algorithm, an output function,

$$g(x, u) \triangleq \omega_{ib}^b - C_n^b\omega_{ie}^n$$

is devised to incorporate Equation 17 as an additional output of the navigation equations. Hence,

$$g(x,u) = \begin{bmatrix} b_x + \omega_x - \Omega S_L S_\theta - \Omega C_L C_\psi C_\theta \\ b_y + \omega_y + \Omega C_L(C_\phi S_\psi - S_\phi S_\theta C_\psi) + \Omega S_L S_\phi C_\theta \\ b_z + \omega_z - \Omega C_L(S_\phi S_\psi + C_\phi S_\theta C_\psi) + \Omega S_L C_\phi C_\theta \end{bmatrix} \qquad (18)$$

where where $C_x \triangleq \cos x$ and $S_x \triangleq \sin x$. Equation 18 is clearly a function of the system states. The Jacobian of Equation 18 is also computed numerically in order to obtain the $H_k$ matrix to be used in the EKF routine.

As in the ZUPT case, consider the scenario described in Section 2.2. The initial navigation states given in Equation 9 constitute the initial estimate of the EKF. The ideal sensor outputs are given in Equations 10 and 11, and the vehicle is assumed to be equipped with a tactical grade IMU as in Section 2.2. At the initialization of the simulations, bias values are determined and are kept constant throughout the simulations.

ZTUPT algorithm assumes no knowledge of the position and attitude of the vehicle. The information available to the algorithm are

$$\begin{bmatrix} v_N \\ v_E \\ v_D \end{bmatrix} = \begin{bmatrix} 0 \\ 0 \\ 0 \end{bmatrix} \quad \text{and} \quad \begin{bmatrix} \dot{\phi} \\ \dot{\theta} \\ \dot{\psi} \end{bmatrix} = \begin{bmatrix} 0 \\ 0 \\ 0 \end{bmatrix}$$

Therefore, the auxiliary sensor output provided to the EKF with ZTUPT is

$$\tilde{y}_k = [v_N \ v_E \ v_D \ \dot{\phi} \ \dot{\theta} \ \dot{\psi}]^T = 0$$

Similar to the ZUPT case, please note that $\tilde{y}_k = 0$ is not a sensor measurement, but acts as a constraint. Hence, the associated covariance matrix is zero, i.e. $R_k = \mathbf{0}_{6x6}$.

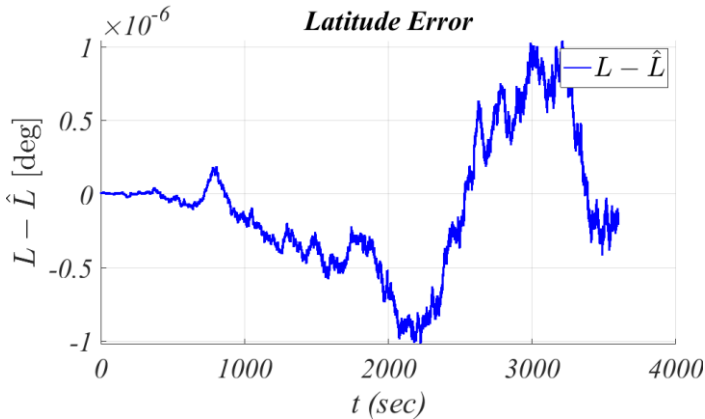Latitude and longitude errors are given in Figures 15 and 16.



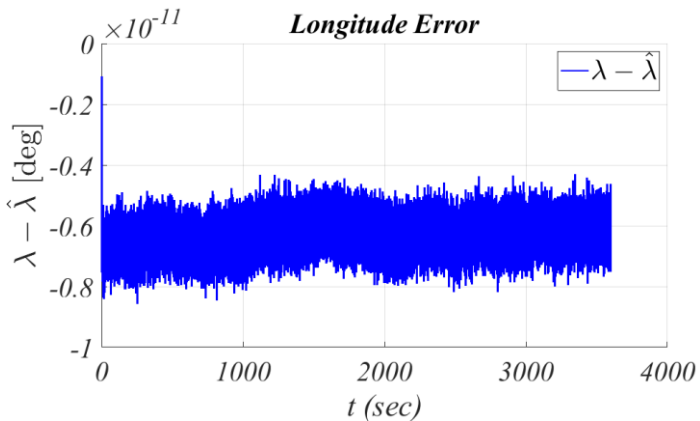*Figure 16. Latitude Error (ZTUPT case)*



*Figure 17. Latitude Error (ZTUPT case)*

Figures 16 and 17 indicate, when the EKF with ZTUPT is active, almost no position error is made. According to the above results, position error is less than 1 m. It is also apparent that the order of magnitude of errors are very similar for both scenarios.
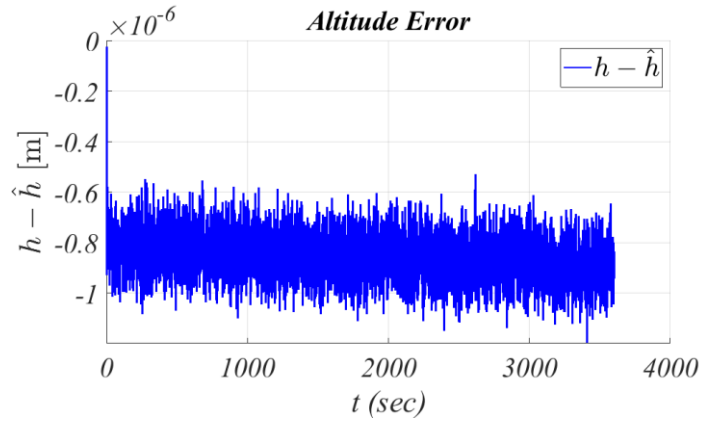


*Figure 18. Altitude Error (ZTUPT case)*

As shown previously in Figure 4 in Section 2.2, altitude diverges when the EKF with ZTUPT is not running. However, the altitude error is virtually nonexistent when the EKF with ZTUPT is active (Figure 18).

Figures for north, east, and down velocities when EKF with ZTUPT is active is not shown here to save space. However, it is stated that the results are as expected and very similar to the results obtained for EKF with ZUPT. The north, east, and down velocities are enforced to remain at zero and the magnitude of error for all three velocities is of order $10^{-21}$.
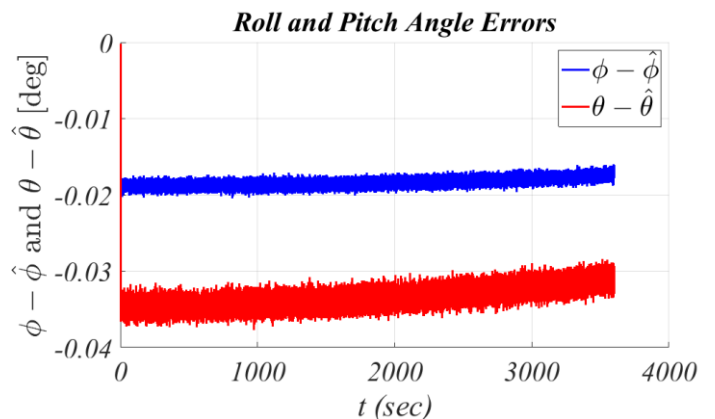


*Figure 19. Roll and Pitch Angle Errors (ZTUPT case)*

Figure 19 shows that the EKF with ZTUPT algorithm bounds roll and pitch angle errors, although –as for the ZUPT case– it cannot drive them to zero. This is because the EKF is not given any information on Euler angles, but just the rates of Euler angles. Roll and pitch angles are initially computed with some error; about *-0.02°* for the roll angle and about *-0.035°* for the pitch angle. This error is due to roll and pitch rate bias of the gyroscope and the time required for the convergence of the extended Kalman filter. The smaller the bias, the smaller the error. (As in Figure 14, please note that there is no discontinuity in the computed roll and pitch angles. The seemingly discontinuous behavior is due to the time scale of the plots.) By comparison, this result is better than the scenario without the EKF as shown in Figure 6, however very similar to the result obtained from EKF with ZUPT as shown in Figure 14.

All the results presented so far to demonstrate that the performance of the ZTUPT algorithm are very similar to the

ZUPT algorithm. However, Figure 19 shows one of the expected benefits of the ZTUPT scenario.
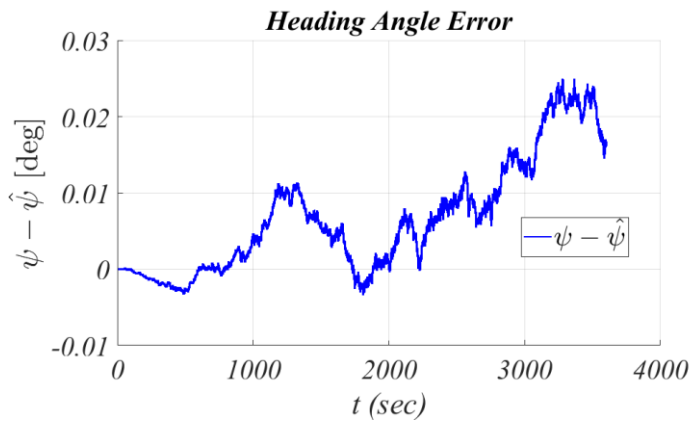


*Figure 19. Heading Angle Error (ZTUPT case)*

Empowered by the information that turn rates are also zero, heading angle errors are successfully bounded by the ZTUPT algorithm. This is an expected result because ZTUPT specifically "tells" the extended Kalman filter that the system is not rotating. Please note that, this result is not the same as North finding. ZTUPT simply prevents the initial heading angle from diverging.

## 4. Summary and Future Work

Two methods that aim to bound navigation errors under GNSS denied environments are discussed in this paper: Zero Velocity Update (ZUPT) and Zero Turning Update (ZTUPT). Both methods show potential in bounding position and velocity errors. However, they are less successful at bounding attitude (Euler angle) errors, although roll and pitch angle error bounds may be deemed acceptable. While the ZUPT method is completely ineffective at bounding heading angle errors, ZTUPT performs much better. Although, estimation of the IMU bias is not the objective of this paper, these methods can be utilized for such a purpose. The main advantage of these methods is the fact that they do not require any additional sensor to be implemented in order to bound the errors. However, they are restrictive in the sense that they only work when the vehicle is not moving, or moving in kinematically constrained manner. Although this is a hard constraint, there are military applications where the position and attitude of a stationary vehicle is of great importance.

This study can be considered as a first step towards utilizing vehicle dynamics as an aiding algorithm to an inertial navigation system. Although, in this paper, a dynamic model is not introduced, properties of a non-moving vehicle are utilized. Reducing navigation errors while at rest is challenging because of the observability issues associated with the linearized dynamics of the system. Additionally, at rest, some of the sensors do measure zero, which makes estimation even harder. In this study, two methods, ZUPT and ZTUPT, are discussed and simulation results are presented. ZUPT manages to bound the navigation errors except for the heading angle. As a matter of fact, ZUPT has no effect on the heading angle. ZTUPT performed better than ZUPT overall, and also managed to bound heading angle errors. Both methods, as expected, failed to drive the attitude states to zero. Future work is going to try to incorporate a vehicle dynamical model and kinematic constraints into the extended Kalman filter structure and investigate the possibility of bounding navigation errors via an implementable framework even when the vehicles in consideration are moving. In addition, future work will incorporate more realistic IMU errors such as scale factor and nonlinearity.

## References

Akcayir, Y. and Ozkazanc, Y. (2003). Gyroscope drift estimation analysis in land navigation systems. In IEEE Conference on Control Applications, volume 2, pages 1488–1491. doi: 10.1109/cca.2003.1223234.

Goshen-Meskin, D. and Bar-Itzhack, I. Y. (1992a). Observability analysis of piece-wise constant systems. i. theory. IEEE Transactions on Aerospace and Electronic Systems, 28(4):1056–1067. doi: 10.1109/7.165367.

Goshen-Meskin, D. and Bar-Itzhack, I. Y. (1992b). Observability analysis of piece-wise constant systems. ii. application to inertial navigation in-flight alignment (military applications). IEEE Transactions on Aerospace and Electronic Systems, 28(4):1068–1075. doi: 10.1109/7.165368.

Groves, Paul D. (2013). Principles of GNSS, inertial, and multisensor integrated navigation systems. Artech House, second edition.

Julier, S. J. and Uhlmann, J. K. (2004). Unscented filtering and nonlinear estimation. Proceedings of the IEEE, 92(3):401–422. doi: 10.1109/jproc.2003.823141.

Ma, H., Yan, L., Xia, Y., and Fu, M. (2020). Kalman filtering and information fusion. Science Press.

Musoff, H. and Zarchan, P. (2009). Fundamentals of kalman filtering: a practical approach. The American Institute of Aeronautics and Astronautics, 3rd edition.

Schmidt, G. T. (2015). Navigation sensors and systems in GNSS degraded and denied environments. Chinese Journal of Aeronautics, 28:1–10. doi: 10.23919/icins.2018.8405890.

Titterton, D. and Weston, J. (2004). Strapdown inertial navigation technology. The American Institute of Aeronautics and Astronautics, 2nd edition.

Wagstaff, B. and Kelly, J. (2018). LSTM-Based zero-velocity detection for robust inertial navigation. In International Conference on Indoor Positioning and Indoor Navigation, pages 1–8. doi: 10.1109/ipin.2018.8533770.

Wahlström, J., Skog, I., Gustafsson, F., Markham, A., and Trigoni, N. (2019). Zero-velocity detection - a bayesian approach to adaptive thresholding. IEEE Sensors Letters, 3(6):1–4. doi: 10.1109/lsens.2019.2917055.

Wan, E. (2006). Sigma-point filters: an overview with applications to integrated navigation and vision assisted control. In IEEE Nonlinear Statistical Signal Processing Workshop, pages 201–202. doi: 10.1109/nsspw.2006.4378854.

Xiaofang, L., Yuliang, M., Ling, X., Jiabin, C., and Chunlei, S. (2014). Applications of zero-velocity detector and Kalman filter in zero velocity update for inertial navigation system. In IEEE Chinese Guidance, Navigation and Control Conference, pages 1760–1763. doi: 10.1109/cgncc.2014.7007449.